

# Constraints on neutrino oscillation parameters from the SNO salt phase data

Abhijit Bandyopadhyay<sup>1</sup>, Sandhya Choubey<sup>2,3</sup>, Srubabati Goswami<sup>4,5</sup>, S.T. Petcov<sup>3,2,6</sup>, D.P. Roy<sup>7</sup>

<sup>1</sup>*Saha Institute of Nuclear Physics, 1/AF, Bidhannagar, Calcutta 700 064, India,*

<sup>2</sup>*INFN, Sezione di Trieste, Trieste, Italy,*

<sup>3</sup>*Scuola Internazionale Superiore di Studi Avanzati, I-34014, Trieste, Italy,*

<sup>4</sup>*Harish-Chandra Research Institute, Chhatnag Road, Jhusi, Allahabad 211 019, India,*

<sup>5</sup>*The Abdus Salam International Centre for Theoretical Physics, I-34100, Trieste, Italy,*

<sup>6</sup>*Institute of Nuclear Research and Nuclear Energy, Bulgarian Academi of Science, Sofia, Bulgaria,*

<sup>7</sup>*Tata Institute of Fundamental Research, Homi Bhabha Road, Mumbai 400 005, India*

## Abstract

The physics implications of the just published salt phase data from the SNO experiment are examined. The effect of these data on the allowed ranges of the solar neutrino oscillation parameters,  $\Delta m_{21}^2$  and  $\sin^2 \theta_{12}$ , are studied in the cases of two- and three- neutrino mixing. In the latter case we derive an upper limit on the angle  $\theta_{13}$ . Constraints on the solar  $\nu_e$  transitions into a mixture of active and sterile neutrinos are also presented. Finally, we give predictions for the day-night asymmetry in the SNO experiment, for the event rate in the BOREXINO and LowNu experiments, and discuss briefly the constraints on the solar neutrino oscillation parameters which can be obtained with prospective KamLAND data.

# 1 Introduction

The past two years have witnessed remarkable experimental progress in the studies of neutrino mixing and oscillations. The latest addition to this magnificent effort is the salt phase data from the SNO experiment [1].

In 2001, the evidences for solar neutrino oscillations [2] obtained in the pioneering experiment of Davis et al. (Homestake) [3, 4], and in the Kamiokande, SAGE, GALLEX/GNO [5] and Super-Kamiokande [6] experiments, were reinforced by the first results of the SNO experiment on the charged current (CC) reaction on deuterium induced by solar neutrinos [7]. In conjunction with the Super-Kamiokande (SK)  $\nu - e^-$  scattering data, the SNO CC data established the existence of solar  $\nu_e$  flavour conversion with a statistical significance of  $3.3\sigma$ . This conclusion was further corroborated by the 2002 SNO data on the neutral current (NC) reaction on deuterium, caused by solar neutrinos [8]. The combined CC and NC SNO data showed at  $5.3\sigma$  the presence of a nonzero  $\nu_{\mu,\tau}$  and/or  $\bar{\nu}_{\mu,\tau}$  component in the flux of the solar  ${}^8B$  neutrinos reaching the Earth. At each stage, the SNO data enabled one to determine with improved precision the average solar  $\nu_e$  survival probability  $P_{ee}$  from the CC reaction data, and the  ${}^8B$  flux normalisation  $f_B$  from the data on the NC reaction. This in turn led to a diminishing of the allowed regions of values of the two parameters - the neutrino mass squared difference  $\Delta m_{21}^2$  ( $\equiv \Delta m_{\odot}^2$ ) and the mixing angle  $\theta_{12}$  ( $\equiv \theta_{\odot}$ ), characterizing the solar neutrino oscillations. The SNO CC data had the main impact of ruling out the Small Mixing Angle (SMA) MSW [9] solution in conjunction with the SK data [7, 10, 11]. The SNO data from the  $D_2O$  phase<sup>1</sup> showed a clear preference for the Large Mixing Angle (LMA) MSW solution of the solar neutrino problem, disfavoring the relatively low  $\Delta m_{21}^2$  (LOW, QVO) solutions [8, 12]. The first results of the KamLAND experiment [13], under the plausible assumption of CPT-invariance in the lepton sector, established the LMA solution as unique solution of the solar neutrino problem.

The combined two-neutrino oscillation analyses of the solar neutrino and KamLAND data, available before the publication of the SNO salt phase results, identified two distinct solution sub-regions within the LMA solution region at 99% C.L. (see, e.g., [14, 15]). The best fit values of  $\Delta m_{\odot}^2$  and  $\theta_{\odot}$  in the two sub-regions - low-LMA and high-LMA, were found to be  $\Delta m_{\odot}^2 = 7.2 \times 10^{-5} \text{ eV}^2$ ,  $\sin^2 \theta_{\odot} = 0.3$ , and  $\Delta m_{\odot}^2 = 1.5 \times 10^{-4} \text{ eV}^2$ ,  $\sin^2 \theta_{\odot} = 0.3$ , respectively [14]. The low-LMA solution was preferred statistically by the data. At 99.73% C.L. ( $3\sigma$ ) the two regions merged and one obtained:

$$\Delta m_{\odot}^2 \cong (5.0 - 20.0) \times 10^{-5} \text{ eV}^2, \quad \sin^2 \theta_{\odot} \cong (0.21 - 0.47) . \quad (1)$$

In the case of 3-neutrino mixing, the analysis of the solar neutrino and KamLAND data involves an additional parameter  $\theta_{13}$  - the neutrino mixing angle limited by the CHOOZ and Palo Verde experiments [16]. The precise upper limit on  $\sin^2 \theta_{13}$  depends on the value of  $\Delta m_{31}^2$  - the neutrino mass squared difference responsible for the atmospheric  $\nu_{\mu}$  and  $\bar{\nu}_{\mu}$  oscillations. The preliminary results of an improved analysis of the SK atmospheric neutrino data, performed recently by the SK collaboration, gave [17]

$$1.3 \times 10^{-3} \text{ eV}^2 \lesssim \Delta m_{31}^2 \lesssim 3.1 \times 10^{-3} \text{ eV}^2, \quad 90\% \text{ C.L.}, \quad (2)$$

---

<sup>1</sup>Here, and in the rest of the paper, by  $D_2O$  phase we mean the NC reactions due to the final state neutron capture on deuterium.

Data set used	best-fit parameters		99% C.L. allowed range	
	$\Delta m_{21}^2 / (10^{-5} \text{eV}^2)$	$\sin^2 \theta_{12}$	$\Delta m_{21}^2 / (10^{-5} \text{eV}^2)$	$\sin^2 \theta_{12}$
Cl+Ga+SK+ $D_2O$	6.06	0.29	3.2 – 24.5	0.21 – 0.44
Cl+Ga+SK+salt	6.08	0.28	3.0 – 23.7	0.19 – 0.43
Cl+Ga+SK+ $D_2O$ +salt	6.06	0.29	3.2 – 17.2	0.22 – 0.40
Cl+Ga+SK+ $D_2O$ +KL	7.17	0.3	5.3 – 9.9	0.22 – 0.44
Cl+Ga+SK+ $D_2O$ +salt+KL	7.17	0.3	5.3 – 9.8	0.22 – 0.40

Table 1: The best-fit values of the solar neutrino oscillation parameters, obtained using different combinations of data sets. Shown also are the 99% C.L. (corresponding to  $\Delta\chi^2$  for a 2 parameter fit) allowed ranges of the parameters from the different analyses.

with a best fit value  $\Delta m_{31}^2 = 2.0 \times 10^{-3} \text{ eV}^2$ .

After the KamLAND results the two major issues to be settled with the future solar neutrino and KamLAND data are:

- Resolving the ambiguity between the low-LMA and the high-LMA solutions and thereby obtaining tighter constraints on  $\Delta m_{21}^2$ .
- Constraining further the allowed range of the solar neutrino mixing angle,  $\theta_{12}$ .

In the present article we examine some of the physics implications of the latest salt phase data from SNO [1]. We study, in particular, the effect of these data on the allowed ranges of the solar neutrino oscillation parameters,  $\Delta m_{21}^2$  and  $\sin^2 \theta_{12}$ . This is done in the cases of two- and three-neutrino mixing. In the latter case we obtain an upper limit on the angle  $\theta_{13}$ . Constraints on the solar  $\nu_e$  transitions into a mixture of active and sterile neutrinos, i.e., on the allowed sterile fraction, are also presented. Finally, we give predictions for the day-night asymmetry in the SNO experiment, for the event rate in the BOREXINO and LowNu experiments, and discuss briefly the constraints on the solar neutrino oscillation parameters which can be obtained with future KamLAND data.

## 2 Two-neutrino oscillation analysis

### 2.1 Analysis with global solar neutrino data

In this Section we first perform a two-neutrino oscillation analysis of the global solar data, incorporating the new SNO results. We include the total rates from the radiochemical experiments Cl and Ga (Gallex, SAGE and GNO combined) [5] and the 1496 day 44 bin SK Zenith angle spectrum data [6]<sup>2</sup>. For SNO we take the combined CC, NC and Electron Scattering (ES) 34 bin energy spectrum data from the  $D_2O$  phase [8], and the recently reported CC, NC and ES rates

<sup>2</sup>SK has recently reanalyzed their day/night data with improved precision [18]. However, the information content in [18] is not enough for including it in our analysis.

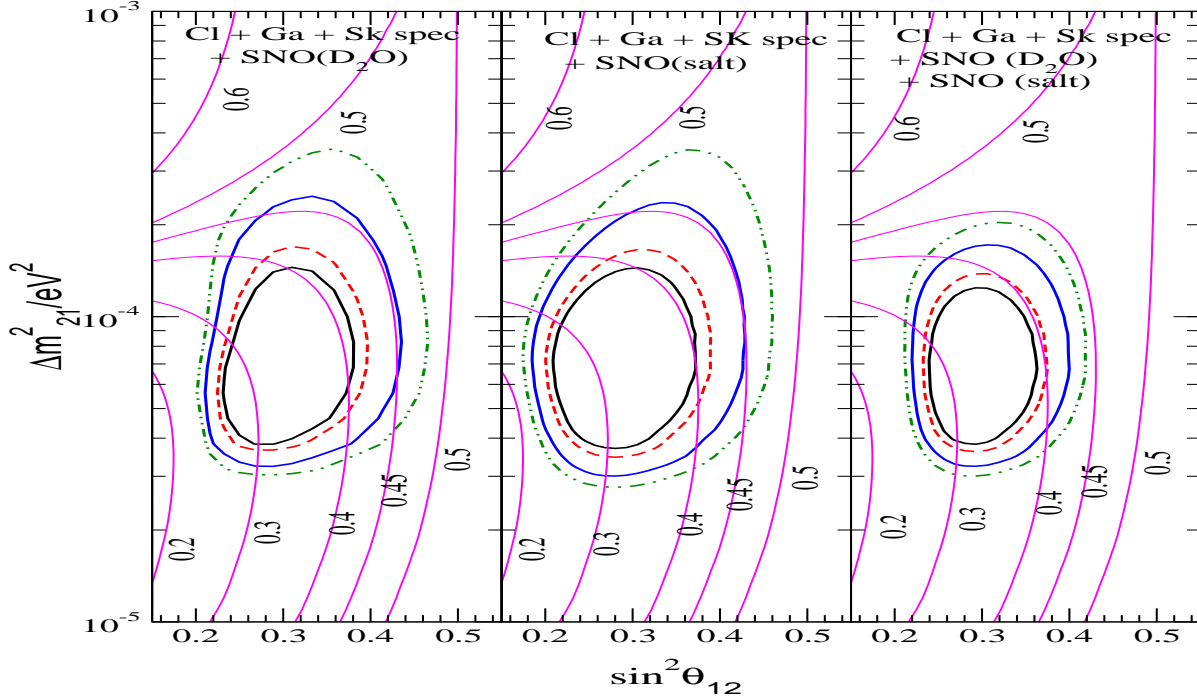


Figure 1: The 90%, 95%, 99% and 99.73% C.L. allowed regions in the  $\Delta m_{21}^2 - \sin^2 \theta_{12}$  plane from global  $\chi^2$ -analysis of the data from solar neutrino experiments. We use the  $\Delta\chi^2$  values corresponding to a two parameter fit to plot the C.L. contours. Also shown are the lines of constant CC/NC event rate ratio  $R_{CC/NC}$ .

from the latest salt phase of the experiment [1]<sup>3</sup>. To ascertain the impact of the salt phase data and facilitate comparison between the impact of the data from the different phases, the SNO data is included in the following three ways in our analysis:

1. Use only the CC+ES+NC day/night spectra data from the  $D_2O$  phase,
2. Use only the CC, ES and NC event rate data from the salt phase,
3. Use data from both phases together.

We follow the instructions given in [19] by the SNO Collaboration in treating the SNO data.

<sup>3</sup>Note that the salt enriched data from SNO gives the CC, ES and NC total rates without any assumption on the  $^8B$  spectrum shape.

For our statistical analysis of the global solar neutrino data we follow a covariant approach and minimise the  $\chi^2$  defined as

$$\chi_{\odot}^2 = \sum_{i,j=1}^N (R_i^{\text{expt}} - R_i^{\text{theory}})(\sigma_{ij}^2)^{-1}(R_j^{\text{expt}} - R_j^{\text{theory}}) \quad (3)$$

where  $R_i$  are the solar data points,  $N$  is the number of data points and  $(\sigma_{ij}^2)^{-1}$  is the inverse of the covariance matrix, containing the squares of the correlated and uncorrelated experimental and theoretical errors. The  ${}^8B$  flux normalisation factor  $f_B$  is left to vary freely in the analysis. For further details of our solar neutrino data analysis we refer the reader to our earlier papers [10, 12].

The results of the analysis of the global solar neutrino data are presented in Table 1 and Figure 1. Table 1 gives the best-fit points and the allowed range of parameter values. The best-fit for the global analysis, including the complete SNO data from both phases, is obtained at  $\Delta m_{21}^2 = 6.06 \times 10^{-5} \text{ eV}^2$ ,  $\sin^2 \theta_{12} = 0.29$  and  $f_B = 1.04$ . Note that if we consider only the salt phase data from SNO, the best-fit value of  $\sin^2 \theta_{12}$  is marginally lower.

In the left panel of Figure 1 we show the allowed region in the parameter space when only the spectrum data from the  $D_2O$  phase are included. In the middle panel the allowed region, obtained by including the SNO salt phase data but excluding the SNO spectrum data from the  $D_2O$  phase, is presented. A comparison of the two panels shows that with the exclusion of the  $D_2O$  phase spectrum data, the allowed region enlarges in size. Even though the SNO data from the  $D_2O$  phase agrees remarkably well with the salt phase data, the ratio of CC and NC event rates,  $R_{CC/NC}$ , is slightly different for the two phases. In particular, for the  $D_2O$  phase, if one uses the data given by SNO for the null hypothesis, one gets for the ratio  $R_{CC/NC} = 0.346$ . For the salt phase, the ratio is  $R_{CC/NC} = 0.306$ . Thus, the CC to NC event rate ratio has decreased, which has very important implications in constraining  $\sin^2 \theta$  and  $\Delta m^2$  [20, 21] (see also [22]). In Figure 1 the iso- $R_{CC/NC}$  contour lines are superimposed on the allowed regions in the  $\Delta m_{21}^2 - \sin^2 \theta_{12}$  plane. The figure clearly shows that since the  $R_{CC/NC}$  for the salt phase data is lower, the allowed regions shift left, following the iso- $R_{CC/NC}$  contours. This results in the shift of the allowed range of  $\sin^2 \theta_{12}$  to smaller values (see Table 1). The allowed  $\Delta m_{21}^2$  shift to lower values as well for the same reason.

The third panel shows the allowed regions, obtained by including the SNO data from both the  $D_2O$  phase and the salt phase. Following the SNO collaboration [19], we treat these two phases as separate experiments with no correlation between them. Combination of the salt phase and the  $D_2O$  phase data produce a more restrictive upper bound on  $\Delta m_{21}^2 \leq 1.7 \times 10^{-4} \text{ eV}^2$  (99.73% C.L.). The upper limit on  $\sin^2 \theta_{12}$  also improves compared to what we have before the salt phase data, as can be seen by comparing the first panel with the last one in Figure 1. The exact intervals in which the solar neutrino oscillations parameters are constrained to lie are given in Table 1.

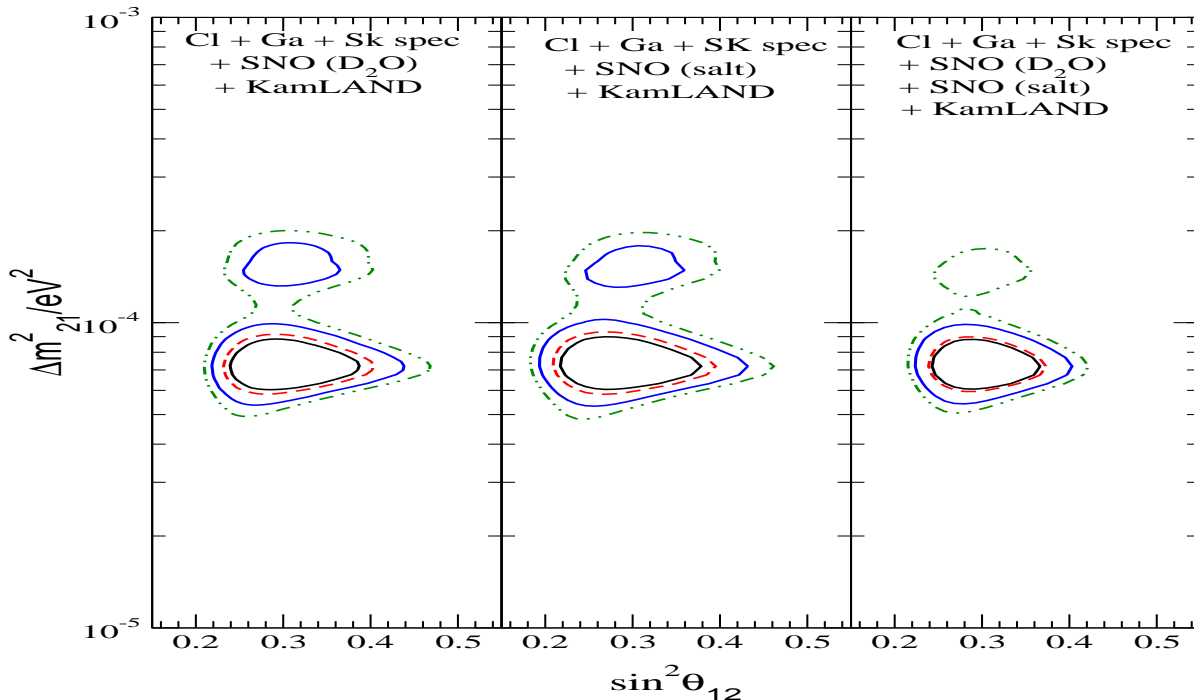


Figure 2: The 90%, 95%, 99% and 99.73% C.L. allowed regions in the  $\Delta m_{21}^2 - \sin^2 \theta_{12}$  plane from global  $\chi^2$ -analysis of solar and KamLAND data. We use the  $\Delta\chi^2$  values corresponding to a 2 parameter fit to plot the C.L. contours.

## 2.2 Constraints from combined solar and KamLAND data

We next include the 162 ton-year results from the KamLAND experiment in the analysis. We use the 13 bin KamLAND spectrum data and defined a  $\chi^2$  assuming a Poissonian distribution as

$$\chi_{klspec}^2 = \sum_i \left[ 2(X_n S_{KL,i}^{theory} - S_{KL,i}^{expt}) + 2S_{KL,i}^{expt} \ln\left(\frac{S_{KL,i}^{expt}}{X_n S_{KL,i}^{theory}}\right) \right] + \frac{(X_n - 1)^2}{\sigma_{sys}^2} \quad (4)$$

where  $\sigma_{sys}$  is taken to be 6.42% and  $X_n$  allowed to vary freely (see [14] for the details of the analysis). In the last 2 rows of Table 1 we give the best-fit data points and the allowed ranges of the parameters obtained before and after including the latest salt phase SNO data in the global analysis. The best-fit point for the combined global analysis is in the low-LMA region at  $\Delta m_{21}^2 = 7.17 \times 10^{-5} \text{ eV}^2$  and  $\sin^2 \theta_{12} = 0.30$ . Thus, the best-fit values of the parameters for

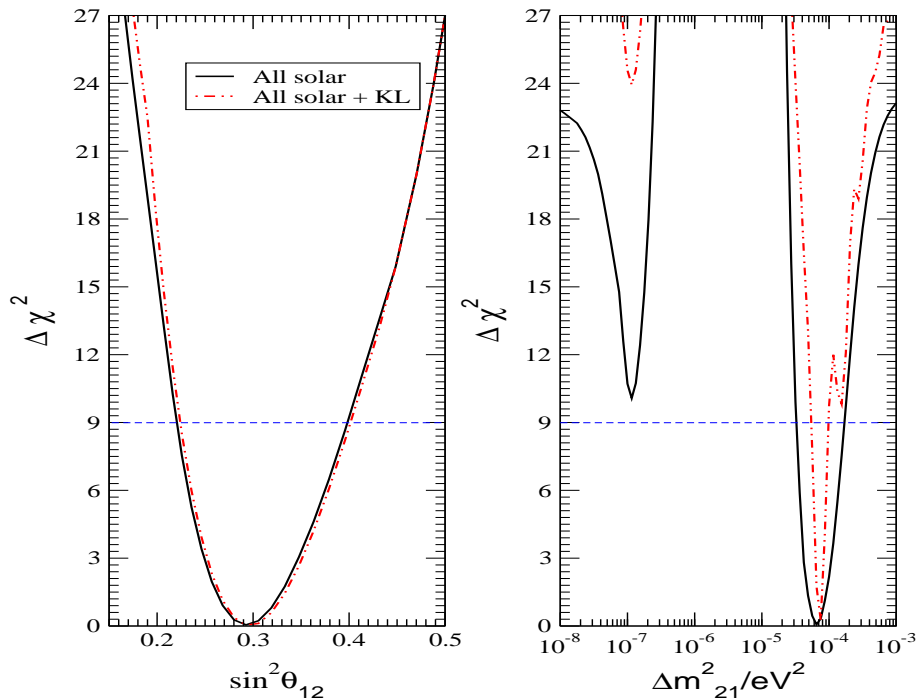


Figure 3: Bounds on  $\Delta m_{21}^2$  and  $\sin^2 \theta_{12}$  from the  $\Delta\chi^2$  as a function of  $\Delta m_{21}^2$  and  $\sin^2 \theta_{12}$ , respectively. The results shown in both panels are obtained by allowing all the other parameters to vary freely. The dashed line shows the  $3\sigma$  limit corresponding to 1 parameter fit.

the combined solar+KamLAND data analysis do not change after inclusion of the latest SNO results. The inclusion of the salt data results in an improvement in the precision of the  ${}^8B$  flux normalisation from  $f_B = 1.01_{-0.19}^{+0.19}$ , obtained without the salt phase data, to  $f_B = 1.02_{-0.15}^{+0.14}$  ( $3\sigma$  results). The agreement with the Standard Solar Model prediction [23] is excellent.

In Figure 2 we present the corresponding allowed regions. Again we show results separately for only the  $D_2O$  phase (left-hand panel), only the salt phase (middle panel) and the global data, with the two phases combined (right-hand panel). Note the shift of the allowed regions in the middle panel which includes only the salt phase data, to smaller values of  $\sin^2 \theta_{12}$ . We find that the separate inclusion of the data from each phase of SNO, in the combined analysis with the KamLAND data, allows the high-LMA solution at 99% C.L.. However when the global solar neutrino data – with data from both phases of SNO combined – is included with the KamLAND data, the high-LMA region is allowed only at 99.13% C.L. ( $2.63\sigma$ ) corresponding to a difference of  $\chi^2$

of 9.5, with respect to the global  $\chi^2_{min}$  obtained in the low-LMA region.

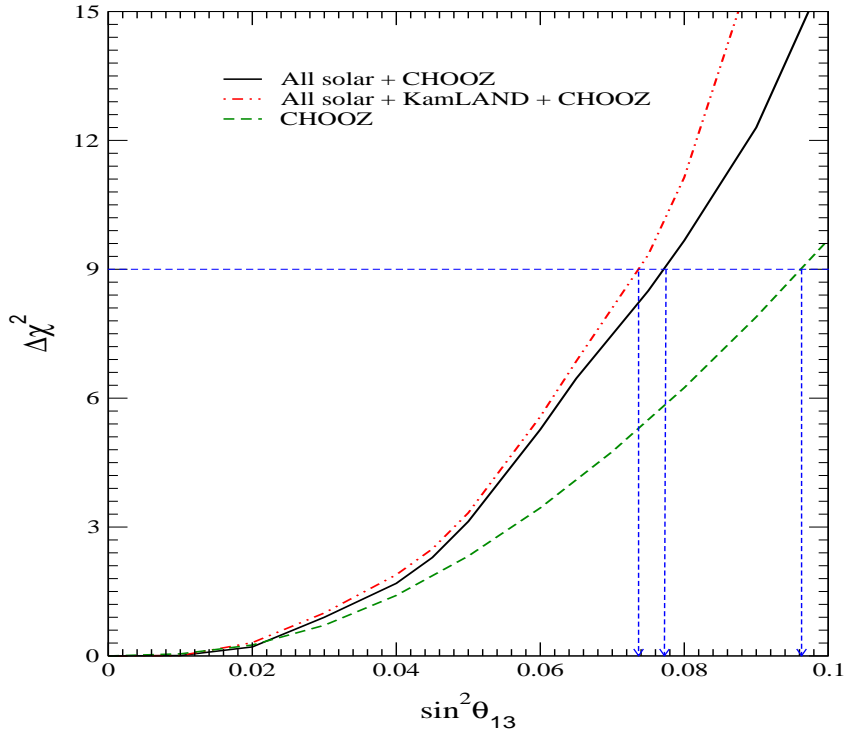


Figure 4: Bounds on the mixing angle  $\theta_{13}$  from the CHOOZ data only (dashed line), the global solar neutrino and CHOOZ data (solid line), and the combined solar, CHOOZ and KamLAND data (dot-dashed line). The  $\Delta m_{31}^2$  is allowed to vary freely within the  $3\sigma$  range ( $2.0_{-0.9}^{+1.2} \times 10^{-3} \text{ eV}^2$ ), which is obtained using the updated SK and K2K results [24]. All the other parameters are allowed to vary freely. The short-dashed line shows the  $3\sigma$  limit corresponding to the case of 1 parameter fit.

In Figure 3 we show the dependence of  $\Delta\chi^2 = \chi^2 - \chi^2_{min}$  on  $\Delta m_{21}^2$  and  $\sin^2\theta_{12}$  respectively, after marginalising over the remaining free parameters. The solid lines represent the  $\Delta\chi^2$  for the global solar neutrino data, while the dot-dashed curves correspond to the combined solar and KamLAND data. We note that the  $\Delta m_{21}^2$  corresponding to the LOW solution is ruled out at slightly more than  $3\sigma$  by the solar neutrino data alone, and at nearly  $5\sigma$  from the combined solar and KamLAND data. KamLAND results are seen to produce a remarkable constraint on  $\Delta m_{21}^2$ . Maximal mixing is now ruled out at more than  $5\sigma$  level by the solar data alone. The KamLAND data does not put a strong constraint on  $\sin^2\theta_{12}$ .

### 3 Bounds from three-neutrino oscillation analysis

So far we have presented results obtained in the framework of two-neutrino oscillations, where the solar  $\nu_e$  oscillates into another active neutrino with a different flavor. However, if the mixing angle  $\theta_{13}$  which is restricted by the CHOOZ and Palo Verde data is not zero, the solar  $\nu_e$  oscillations will involve also the third heaviest neutrino mass eigenstate, with the associated neutrino mass squared difference given by  $\Delta m_{31}^2$ . The relevant electron neutrino/antineutrino survival probability in the three-neutrino mixing case is given by the following expression:

$$P_{ee}^{3gen} \cong \cos^4 \theta_{13} P_{ee}^{2gen} + \sin^4 \theta_{13} \quad (5)$$

where  $P_{ee}^{2gen}$  is the  $\nu_e$  survival probability for two-neutrino mixing (see, e.g., [25]). In the case of solar neutrinos,  $P_{ee}^{2gen} \equiv P_{ee\odot}^{2gen}$  is the two-neutrino oscillation  $\nu_e$  survival probability [26] with the solar electron number density  $N_e$  replaced by  $N_e \cos^2 \theta_{13}$ . The term  $\sin^4 \theta_{13}$  can be neglected to a good approximation in eq. (5). Since for the solar neutrinos one has  $P_{ee\odot}^{2gen} \approx \sin^2 \theta_{12}$  in the low-LMA region, we have  $P_{ee\odot}^{3gen} \approx \cos^4 \theta_{13} \sin^2 \theta_{12}$ . For the reactor  $\bar{\nu}_e$  detected in the KamLAND experiment, the matter effects are negligible and one gets  $P_{eeKL}^{3gen} = \cos^4 \theta_{13} \{1 - \sin^2 2\theta_{12} \sin^2(\Delta m_{21}^2 L/4E)\}$ , where  $L$  is the source-detector distance and  $E$  the antineutrino energy. As Eq. (5) indicates, the presence of a non-zero  $\theta_{13}$  shifts  $\theta_{12}$  obtained from the two-neutrino oscillation solar neutrino data analysis to larger values. In contrast, for the reactor antineutrinos, one can expect the allowed range of  $\theta_{12}$ , determined from a two-neutrino mixing analysis of the reactor antineutrino data, to shift to smaller values, if  $\theta_{13}$  is non-zero and is sufficiently large. The survival probability for the short-baseline CHOOZ experiment is approximately given by  $P_{eeCHOOZ}^{3gen} \approx 1 - \sin^2 2\theta_{13} \sin^2(\Delta m_{31}^2 L/4E)$  and is hence very sensitive to the range of allowed value of atmospheric neutrino mass squared difference,  $\Delta m_{31}^2$ <sup>4</sup>. Therefore with the shift of  $\Delta m_{31}^2$  to lower values in the new SK analysis, the constraint on  $\theta_{13}$  from CHOOZ is expected to get affected. The information in [17] is not sufficient for a full global analysis using the SK atmospheric data. We adopt the following procedure. We allow  $\Delta m_{31}^2$  to vary freely within the range given in [24], obtained using the updated SK [17] and K2K [28] results and perform a combined three-neutrino oscillation analysis of the global solar neutrino and reactor data, including both the KamLAND and CHOOZ results (for earlier global three generation analyses see, e.g. [29]).

In Figure 4 we present the  $\Delta\chi^2$  obtained for various fixed values of  $\sin^2 \theta_{13}$ , when all other parameters are allowed to vary freely. The  $3\sigma$  bounds on  $\sin^2 \theta_{13}$ , obtained from the global solar neutrino and CHOOZ data analysis, can be directly read from the figure as  $\sin^2 \theta_{13} < 0.077$ . The bound derived from the combined analysis of the solar neutrino, CHOOZ and KamLAND data tightens somewhat to  $\sin^2 \theta_{13} < 0.074$ .<sup>5</sup> As a result of lowering of the  $\Delta m_{31}^2$  range according to the new SK atmospheric neutrino data analysis, the bound obtained from only CHOOZ data weakens: as can be seen from figure 4, this bound reads now as  $\sin^2 \theta_{13} < 0.096$ . We have checked that the marginalised bounds on  $\Delta m_{21}^2$  and  $\sin^2 \theta_{12}$ , even for the three-generation analysis, are the same as those given in Figure 3.

<sup>4</sup>In our numerical calculation we use the probability keeping the  $\Delta m_{21}^2$  terms [27].

<sup>5</sup>If we let  $\Delta m_{31}^2$  to vary within the range allowed by the earlier SK analysis we get  $\sin^2 \theta_{13} < 0.057$ . Thus the ratio of the old and the new bound on  $\sin^2 \theta_{13}$  is 1.3 and this matches with the corresponding results in [24]. We have checked that at each C.L. the value of the old and the new limit differs by this same factor.

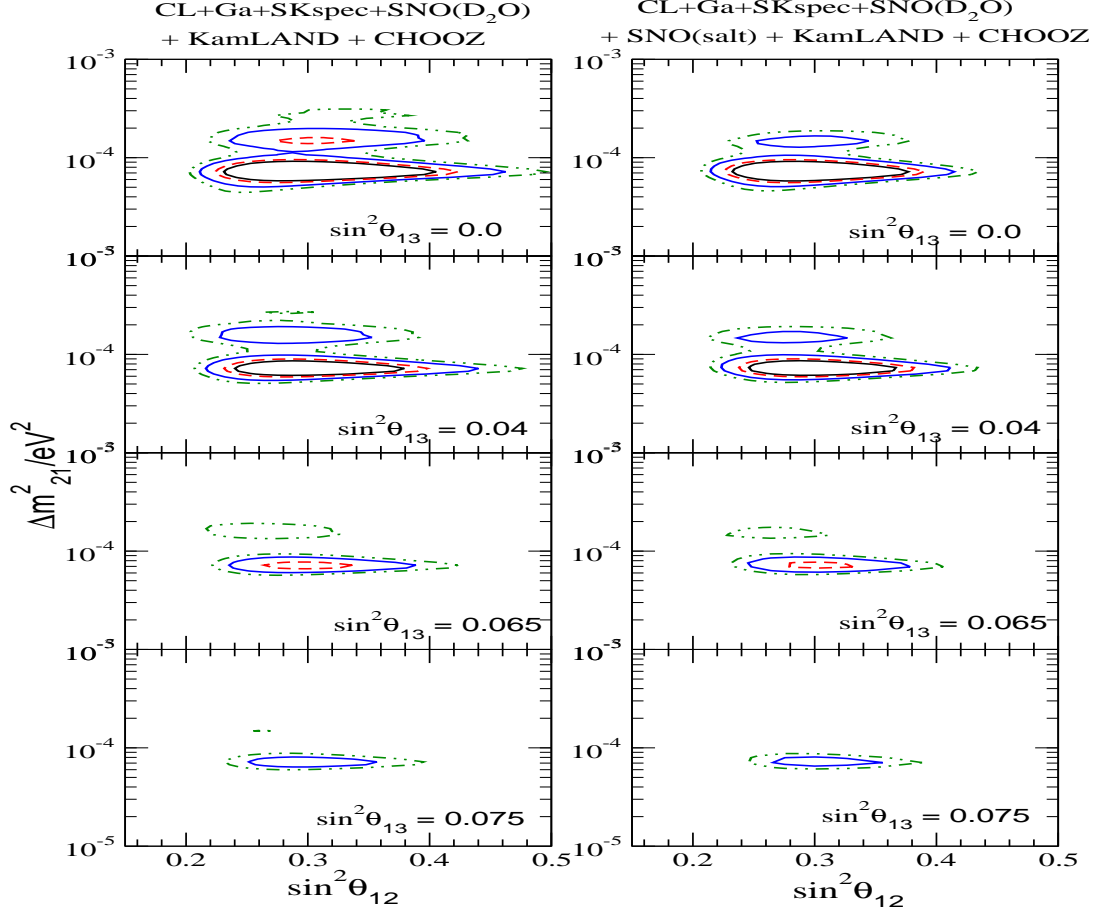


Figure 5: The 90%, 95%, 99% and 99.73% C.L. allowed contours in the  $\Delta m_{21}^2 - \sin^2 \theta_{12}$  plane, from the three-neutrino oscillation analysis of the global solar and reactor data, including the data from the KamLAND and CHOOZ experiments. The different panels are drawn at different fixed values of  $\sin^2 \theta_{13}$ .  $\Delta m_{31}^2$  is allowed to vary freely within appropriate range taken from [24]. The left hand panels are before the SNO salt data while the right hand panels are including the SNO salt data. Here we use three parameter fit  $\Delta\chi^2$  values to plot the C.L. contours.

In Figure 5 we present the allowed regions in the  $\Delta m_{21}^2 - \sin^2 \theta_{12}$  plane, for four fixed values of  $\theta_{13}$  for cases with and without the SNO salt data. With the inclusion of the salt data the allowed regions decrease in size for all values of  $\theta_{13}$ . The presence of a small non-zero  $\theta_{13}$  improves the fit in the regions of the parameter space with higher values of  $\Delta m_{21}^2$ , i.e., in the high-LMA zone, where the  ${}^8B$  neutrino transitions are not affected by matter effects over a part of the energy spectrum [30], and which therefore give a larger value of the CC/NC event rate ratio. The presence of the  $\cos^4 \theta_{13}$  factor in the survival probability acts as a normalisation which effectively reduces the CC event rate and hence makes the high-LMA region less disfavored by the data. Since matter effects in the Sun are relatively small for the high-LMA values of  $\Delta m_{21}^2$ , the allowed regions in these zones appear at smaller values of  $\theta_{12}$ , as discussed above. However, as  $\theta_{13}$  increases, the allowed areas shrink and finally vanish for  $\sin^2 \theta_{13} > 0.075$ . Note that we get allowed regions at  $\sin^2 \theta_{13} = 0.075$  even though from Figure 4 the  $3\sigma$  range appears to be  $\sin^2 \theta_{13} < 0.074$ . This is because in Figure 5 we use a  $\Delta\chi^2$  which corresponds to a three parameter fit.

## 4 Constraints on transitions into a state with a sterile neutrino component

As is well known, the explanation of the positive evidences of oscillations from the LSND [31] experiment and the solar and atmospheric neutrino oscillation data requires the existence of a fourth neutrino which has to be inert [32]. A comparison of the SNO CC and NC data from the  $D_2O$  phase had already ruled out solar  $\nu_e$  oscillations into pure sterile state at  $5.3\sigma$  [8]. The inclusion of the SNO salt phase data raises the degree of disfavour to  $7.8\sigma$  level [1]. However, transitions to “mixed” states, where the final neutrino state is a mixture of active and sterile components, is still allowed by the data. We find the limits on the sterile fraction from the global data. Bounds on allowed fraction of sterile component in the solar  $\nu_e$  flux has earlier been obtained in [33].

We consider a general case where the  $\nu_e$  produced in the Sun transforms into a “mixed” state given by  $\nu' = \sin \alpha \nu_{active} + \cos \alpha \nu_{sterile}$ . Thus,  $\sin^2 \alpha (\cos^2 \alpha)$  gives the fraction of the active (sterile) component in the resultant solar neutrino flux at Earth. In Figure 6 we present the plots of  $\Delta\chi^2$  vs  $f_B$  (left-hand panel), and  $\Delta\chi^2$  vs  $\sin^2 \alpha$  (right-hand panel), allowing the mass and mixing parameters to vary freely in the LMA region. The solid lines show the constraints from the solar data alone, while the dot-dashed lines correspond to the combined solar and KamLAND data. The range of allowed values of  $f_B$ , determined from the global solar (solar+KamLAND) data analysis at  $3\sigma$  is  $0.87 - 1.2$  (1.16). The allowed value for the sterile fraction in the resultant solar neutrino flux at Earth is constrained to  $1 - \sin^2 \alpha < 0.60$  (0.44) at  $3\sigma$  by the solar (solar+KamLAND) data. Before the SNO salt phase data was announced, the corresponding limit for the sterile fraction at  $3\sigma$  from the combined solar+KamLAND data analysis was  $1 - \sin^2 \alpha < 0.54$ . Thus, the SNO salt data is seen to tighten the noose on the possible presence of a sterile component in the solar neutrino flux.

## 5 Future and outlook

With the latest salt phase data from SNO giving further credence to the low-LMA solution, we are entering the era of precision measurements in the field of solar neutrino physics. The high-LMA

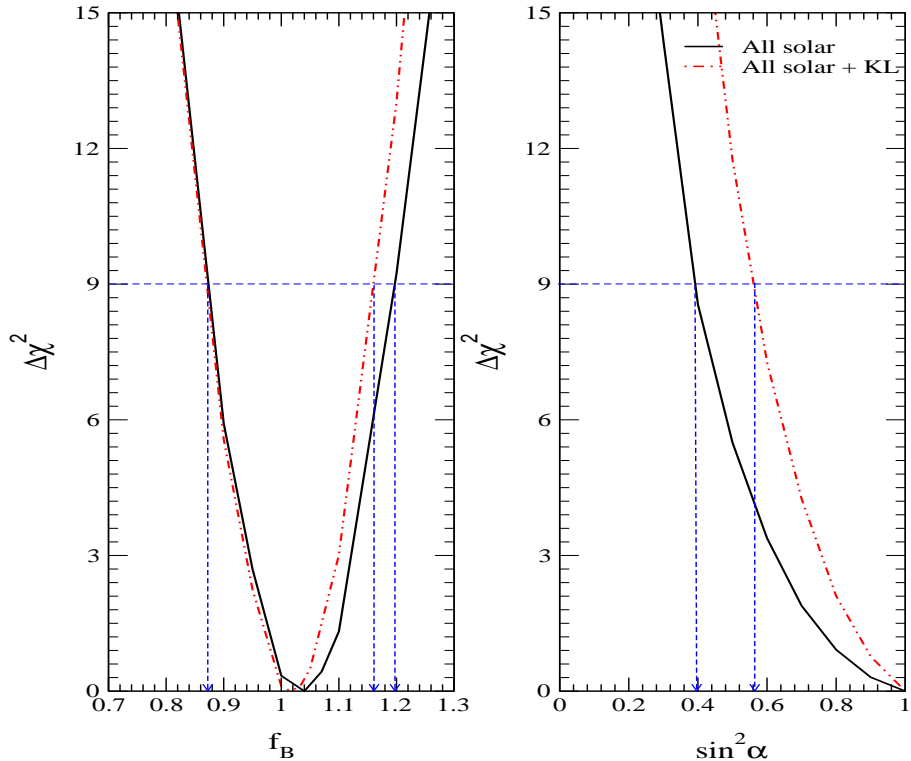


Figure 6: Bounds on  $f_B$  and the sterile fraction in the solar neutrino flux, given by  $1 - \sin^2 \alpha$ . The left panel shows the  $\Delta\chi^2$  as a function of  $f_B$ , while the right-hand panel gives the corresponding bounds on  $\sin^2 \alpha$ . The  $\Delta\chi^2$  is marginalised over all the oscillation parameters. The dashed line shows the  $3\sigma$  limit corresponding to one parameter fit.

solution stands disfavored at more than 99% C.L. and only a small area appears at the  $3\sigma$  level. The next phase of the SNO experiment will be devoted to obtaining neutral current data using Helium counters [34]. This would give a totally uncorrelated information on the CC and NC event rates observed at SNO. In the near future, SNO is expected to provide data on the day/night spectrum, which could be used in a statistical analysis to further constrain the solar neutrino oscillation parameters [21, 35]. One of the related observables is the day-night asymmetry:

$$A_{DN} = 2 \frac{N - D}{N + D}. \quad (6)$$

In Figure 7 we show the lines of constant  $A_{DN}$  for SNO. The predicted  $A_{DN}$  in SNO, for the current best-fit values of the parameters in the low-LMA region, as well as the corresponding  $3\sigma$

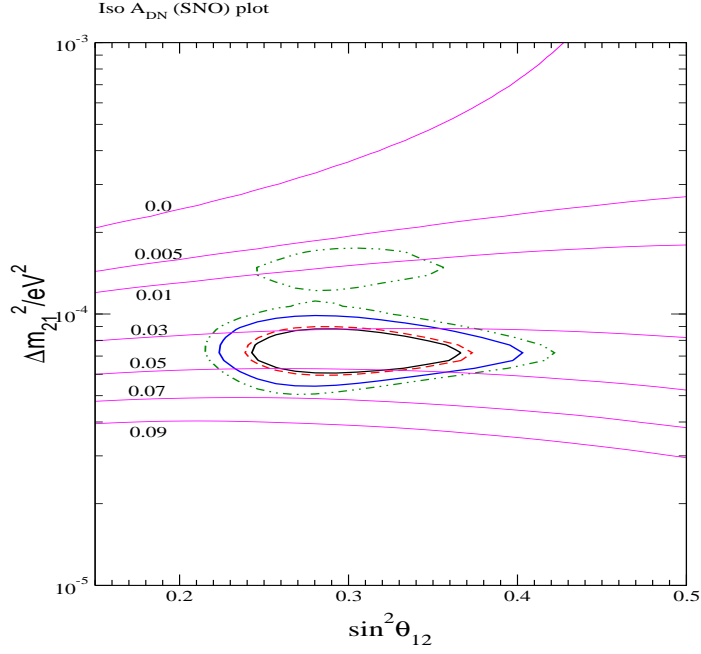


Figure 7: Lines of constant day-night asymmetry for the SNO experiment, superposed on the allowed region from the global analysis of the solar and KamLAND data.

range, are given by

$$A_{DN}^{SNO} = 0.04, \quad 3\sigma \text{ range : } 0.02 - 0.07, \quad \text{low - LMA}, \quad (7)$$

For the barely allowed high-LMA solution we get:

$$A_{DN}^{SNO} = 0.01, \quad 3\sigma \text{ range : } 0.007 - 0.02, \quad \text{high - LMA}. \quad (8)$$

The potential of Borexino [36] and any generic electron scattering experiment for the low energy  $pp$  neutrinos – the LowNu experiments [37] – in constraining the mass and mixing parameters have been studied most recently in [38, 39]. For the allowed regions obtained in the current paper, we find the predicted rates for Borexino and LowNu experiments to be

$$R_{Be} = 0.65, \quad (3\sigma \text{ range } \equiv 0.61 - 0.71); \quad \text{low - LMA} \quad (9)$$

$$R_{pp} = 0.71, \quad (3\sigma \text{ range } \equiv 0.67 - 0.76); \quad \text{low - LMA} \quad (10)$$

High precision measurement results can be expected from the reactor experiment KamLAND [40]. With statistics of 1 kTy, the KamLAND data could reduce the uncertainty in the  $\Delta m_{21}^2$  determination to a few percent [38]. In Figures 8 and 9 we present the two-neutrino mixing allowed regions in the  $\Delta m_{21}^2 - \sin^2 \theta_{12}$  plane, obtained from a combined analysis of the current global solar neutrino data and a prospective 0.41 kTy<sup>6</sup> and 1 kTy simulated data in KamLAND.

<sup>6</sup>This corresponds to 2.5 times the statistics of the first published data from KamLAND.

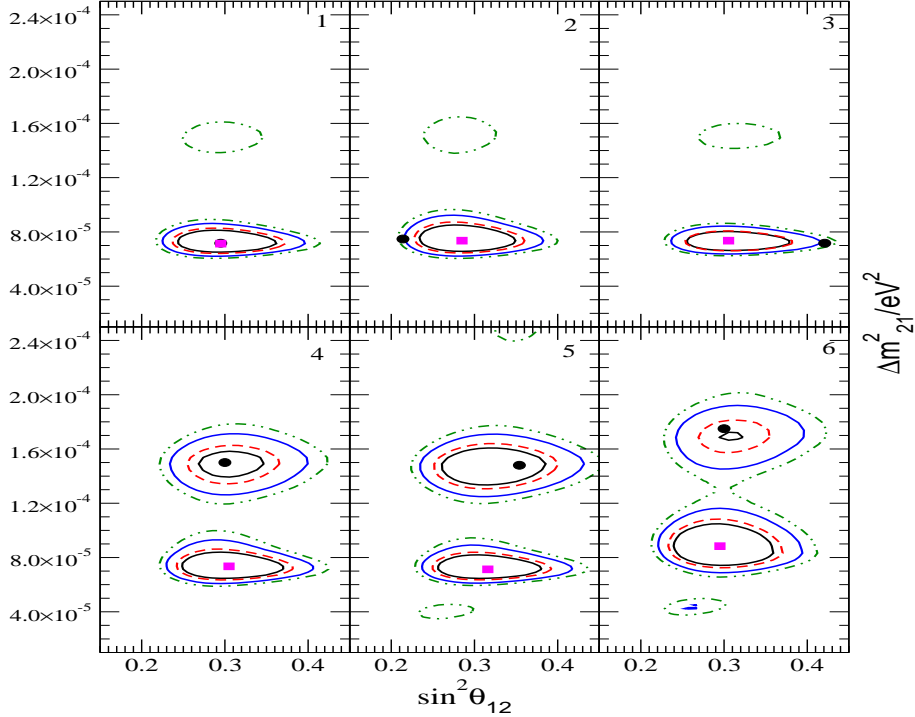


Figure 8: The 90%, 95%, 99% and 99.73% C.L. allowed regions obtained from a combined analysis using the global solar neutrino data and a 0.41 kTy simulated KamLAND data. The points in the parameter space, for which the 0.41 kTy KamLAND data has been simulated, are shown by the dots; they have been chosen to lie within the current  $3\sigma$  allowed regions. The best-fit point of the combined analysis are shown as “boxes”.

Since in future the systematic uncertainty in KamLAND data is expected to be reduced (especially with the fiducial volume calibration), we use a value of 5% for the KamLAND systematic error in this analysis. The black dots in the various panels of Figures 8 and 9 denote the point in the parameter space, for which the data has been simulated. The pink squares give the best-fit points obtained in the joint analysis. For the upper row of panels, the points at which we simulate the KamLAND data lie in the low-LMA region. We note that if the true solution lies in the low-LMA region, a spurious high-LMA solution still appears at  $3\sigma$  level in the case of 0.41 kTy of statistics, though the allowed area gets further reduced in size, owing to the precision of the KamLAND data. The high-LMA solution disappears if the statistics is increased to 1.0 kTy. For all the panels the precision on the range of allowed value of  $\Delta m_{21}^2$  is seen to improve. There is little improvement, however, in the precision of  $\sin^2 \theta_{12}$  [38, 41]. One expects a significant improvement

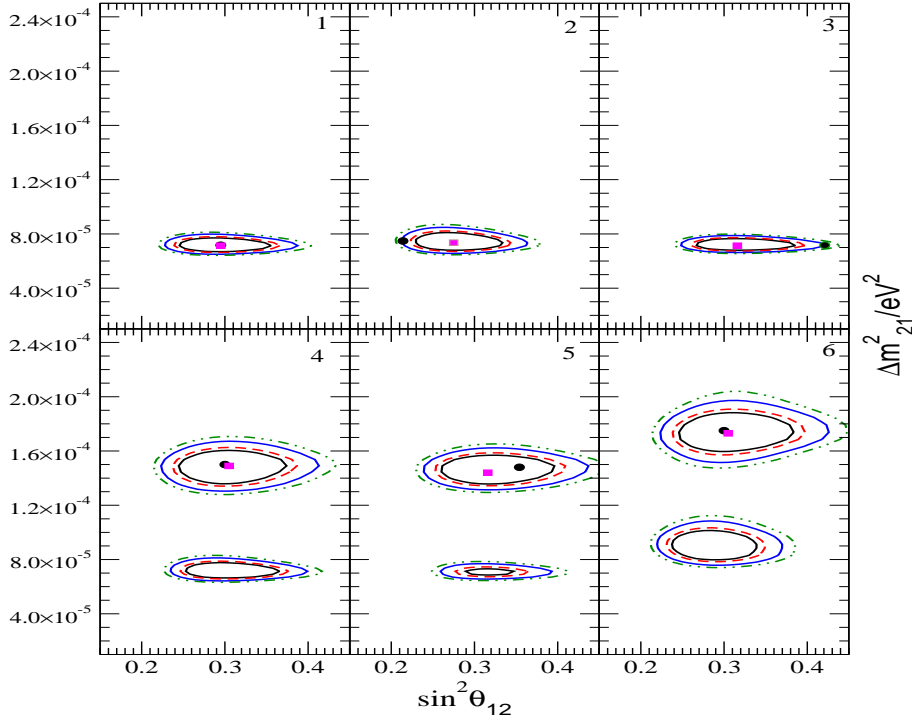


Figure 9: Same as Fig. 8, but for 1 kTy statistics.

in the precision of  $\sin^2 \theta_{12}$  over the low-LMA region to come from a more precise measurement [42] of the CC/NC ratio at the next phase of SNO. In the lower row of Figures 8 and 9 we illustrate a scenario that would show itself if the future KamLAND data conforms to a point in the high-LMA region. Since the low-LMA solution is now strongly favored over the high-LMA one by the global solar neutrino data, if such a contradictory situation arises whereby the KamLAND data alone would favor the high-LMA solution, both solutions would get allowed and the solution ambiguity would remain. As can be seen in the last row panels of Figures 8 and 9, the best-fit point comes in the low-LMA (high-LMA) region for 0.41 kTy (1 kTy) statistics. We have checked that if we simulate the spectrum in the high-LMA region, the best-fit shifts from the low-LMA to the high-LMA region after KamLAND collects about 1 kTy statistics.

## 6 Conclusions

We analysed the impact of the salt phase data from the SNO experiment in global solar neutrino oscillation analysis, including the KamLAND data as well. The inclusion of the CC and NC event rates from the SNO salt phase data strongly favours  $\Delta m_{21}^2$  to lie in the low-LMA region.

Values of  $\Delta m_{21}^2$  in the LOW area get disfavoured at more than  $3\sigma$  just from global solar neutrino data, and at almost  $5\sigma$  from the combined solar and KamLAND data. The combined effect of the SNO spectrum data from the  $D_2O$  phase and of the data from the salt phase results in lowering the upper bound on  $\Delta m_{21}^2$  to  $\Delta m_{21}^2 \leq 1.7 \times 10^{-4} \text{ eV}^2$  (99.73% C.L.). The global solar + KamLAND data still admit the high-LMA solution, but it appears only at  $2.63\sigma$  level. The addition of the new SNO data restricts the mixing angle  $\theta_{12}$  from above and maximal mixing is now excluded at more than  $5\sigma$ . With the inclusion of non-zero values of the mixing angle  $\theta_{13}$  in a 3-neutrino mixing analysis, the allowed regions in the  $\Delta m_{21}^2 - \sin^2 \theta_{12}$  plane decrease in size as  $\theta_{13}$  increases. At  $\sin^2 \theta_{13} \geq 0.075$  no allowed regions are obtained at 99.73% C.L. The solution due to transitions into sterile neutrino is excluded at  $7.8\sigma$  with the salt phase data. However, solar  $\nu_e$  transitions into a mixed sterile + active state are allowed, with the sterile fraction restricted to be  $< 44\%$  at  $3\sigma$ . With the knowledge of  $\Delta m_{21}^2$  and  $\sin^2 \theta_{12}$  responsible for the solar neutrino oscillations becoming more precise, the predicted ranges for the day-night asymmetry in SNO, and of the event rates in Borexino and the LowNu, experiments narrow down. We also studied the impact of the prospective increase in statistics of the KamLAND data, on the determination of the solar neutrino oscillation parameters. If the spectrum is simulated at a point in the low-LMA region, the allowed  $3\sigma$  area in the high-LMA zone reduces in size in the case of 0.41 kTy of data, and disappears if the statistics is increased to 1.0 kTy. If, however, the KamLAND spectrum corresponds to a point in the high-LMA zone, the conflicting trend of solar and KamLAND data would make the high-LMA solution reappear at 90% C.L. and the determination of  $\Delta m_{21}^2$  would remain ambiguous.

The authors would like to thank E. Lisi for clarifying comments concerning ref. [24]. S.G. would like to thank The Abdus Salam International Centre for Theoretical Physics for hospitality.

## References

- [1] S. N. Ahmed *et al.* [SNO Collaboration], arXiv:nucl-ex/0309004.
- [2] B. Pontecorvo, *Zh. Eksp. Teor. Fiz.* **53** (1967) 1717.
- [3] B. Pontecorvo, Chalk River Lab. report PD-205, 1946.
- [4] R. Davis, D.S. Harmer and K.C. Hoffman, *Phys. Rev. Lett.* **20**, 1205 (1968); R. Davis, Proc. of the “Neutrino ‘72” Int. Conference, Balatonfured, Hungary, June 1972 (eds. A. Frenkel and G. Marx, OMKDK-TECHNOINFORM, Budapest, 1972), p.5.
- [5] B. T. Cleveland *et al.*, *Astrophys. J.* **496**, 505 (1998); J. N. Abdurashitov *et al.* [SAGE Collaboration], *J. Exp. Theor. Phys.* **95**, 181 (2002) [*Zh. Eksp. Teor. Fiz.* **122**, 211 (2002)] [arXiv:astro-ph/0204245]; W. Hampel *et al.* [GALLEX Collaboration], *Phys. Lett. B* **447**, 127 (1999); E. Bellotti, Talk at Gran Sasso National Laboratories, Italy, May 17, 2002; T. Kirsten, talk at *Neutrino 2002*, XXth International Conference on Neutrino Physics and Astrophysics, Munich, Germany, May 25-30, 2002. (<http://neutrino2002.ph.tum.de/>).

- [6] S. Fukuda *et al.* [Super-Kamiokande Collaboration], Phys. Lett. B **539**, 179 (2002) [arXiv:hep-ex/0205075].
- [7] Q. R. Ahmad *et al.* [SNO Collaboration], Phys. Rev. Lett. **87**, 071301 (2001) [arXiv:nucl-ex/0106015].
- [8] Q. R. Ahmad *et al.* [SNO Collaboration], Phys. Rev. Lett. **89**, 011301 (2002) [arXiv:nucl-ex/0204008]; Q. R. Ahmad *et al.* [SNO Collaboration], Phys. Rev. Lett. **89**, 011302 (2002) [arXiv:nucl-ex/0204009].
- [9] L. Wolfenstein, Phys. Rev. D **17**, 2369 (1978) ; S. P. Mikheev and A. Y. Smirnov, Sov. J. Nucl. Phys. **42** (1985) 913 [Yad. Fiz. **42**, 1441 (1985)].
- [10] A. Bandyopadhyay, S. Choubey, S. Goswami and K. Kar, Phys. Lett. B **519**, 83 (2001) [arXiv:hep-ph/0106264].
- [11] G.L. Fogli, E. Lisi, D. Montanino, A. Palazzo, Phys. Rev. **D64**, 093007 (2001); J.N. Bahcall, M.C. Gonzalez-Garcia, C. Pana-Garay, JHEP **0108**, 014 (2001); P. I. Krastev and A. Y. Smirnov, Phys. Rev. D **65**, 073022 (2002) [arXiv:hep-ph/0108177]; M.V. Garzelli and C. Giunti, JHEP **0112**, 017 (2001).
- [12] A. Bandyopadhyay, S. Choubey, S. Goswami and D. P. Roy, Phys. Lett. B **540**, 14 (2002) [arXiv:hep-ph/0204286]; S. Choubey, A. Bandyopadhyay, S. Goswami and D. P. Roy, arXiv:hep-ph/0209222 and references therein.
- [13] K. Eguchi *et al.* [KamLAND Collaboration], Phys. Rev. Lett. **90**, 021802 (2003) [arXiv:hep-ex/0212021].
- [14] A. Bandyopadhyay, S. Choubey, R. Gandhi, S. Goswami and D. P. Roy, Phys. Lett. B **559**, 121 (2003) [arXiv:hep-ph/0212146].
- [15] G. L. Fogli *et al.*, Phys. Rev. D **67**, 073002 (2003) [arXiv:hep-ph/0212127]; M. Maltoni, T. Schwetz and J. W. Valle, Phys. Rev. D **67**, 093003 (2003) [arXiv:hep-ph/0212129]; J. N. Bahcall, M. C. Gonzalez-Garcia and C. Pena-Garay, JHEP **0302**, 009 (2003) [arXiv:hep-ph/0212147]; H. Nunokawa, W. J. Teves and R. Zukanovich Funchal, Phys. Lett. B **562**, 28 (2003) [arXiv:hep-ph/0212202]; P. Aliani *et al.*, arXiv:hep-ph/0212212; P. C. de Holanda and A. Y. Smirnov, JCAP **0302**, 001 (2003) [arXiv:hep-ph/0212270].
- [16] M. Apollonio *et al.*, Phys. Lett. **B466** (1999) 415; F. Boehm *et al.*, Phys. Rev. **D62** (2000) 072002.
- [17] Super-Kamiokande Coll., Y. Hayato *et al.*, Talk given at the Int. EPS Conference on High Energy Physics, July 17 - 23, 2003, Aachen, Germany.
- [18] [Super-Kamiokande Collaboration], arXiv:hep-ex/0309011.

- [19] “HOWTO use the SNO Salt Flux Results”, and “HOWTO use the SNO Solar Neutrino Spectral data”, SNO Collaboration, <http://www.sno.phy.queensu.ca/>.
- [20] M. C. Gonzalez-Garcia, C. Pena-Garay, Y. Nir and A. Y. Smirnov, Phys. Rev. D **63**, 013007 (2001) [arXiv:hep-ph/0007227].
- [21] M. Maris and S. T. Petcov, Phys. Lett. B **534** (2002) 17 [arXiv:hep-ph/0201087].
- [22] J. N. Bahcall and E. Lisi, Phys. Rev. D **54**, 5417 (1996) [arXiv:hep-ph/9607433]; E. Lisi and D. Montanino, Phys. Rev. D **56** (1997) 1792; J. N. Bahcall, P. I. Krastev and A. Y. Smirnov, Phys. Rev. D **62**, 093004 (2000) [arXiv:hep-ph/0002293]; J.N. Bahcall, P.I. Krastev and A. Y. Smirnov, JHEP 0105 (2001) 015; J.N. Bahcall, M.C. Gonzalez-Garcia and C. Peña-Garay, JHEP 0204 (2002) 007.
- [23] J.N. Bahcall, M.H. Pinsonneault and S. Basu, Astrophys. J. **555**, 990 (2001).
- [24] G. L. Fogli, E. Lisi, A. Marrone, D. Montanino, A. Palazzo and A. M. Rotunno, arXiv:hep-ph/0308055.
- [25] S.T. Petcov, Phys. Lett. B **214**, 259 (1988).
- [26] S.T. Petcov, Phys. Lett. B **200**, 373 (1988), and Phys. Lett. B **214**, 139 (1988); S.T. Petcov and J. Rich, Phys. Lett. B **224**, 401 (1989); P.I. Krastev and S.T. Petcov, Phys. Lett. B **207**, 64 (1988); E. Lisi et al., Phys. Rev. D **63**, 093002 (2000).
- [27] S.M. Bilenky, D. Nicolo and S.T. Petcov, *Phys. Lett.* **B538** (2002) 77.
- [28] M. H. Ahn *et al.* [K2K Collaboration], Phys. Rev. Lett. **90**, 041801 (2003) [arXiv:hep-ex/0212007].
- [29] G. L. Fogli, E. Lisi and D. Montanino, Phys. Rev. D **54**, 2048 (1996) [arXiv:hep-ph/9605273]; M. C. Gonzalez-Garcia, M. Maltoni, C. Pena-Garay and J. W. F. Valle, Phys. Rev. D **63**, 033005 (2001) [arXiv:hep-ph/0009350]; A. Bandyopadhyay, S. Choubey, S. Goswami and K. Kar, Phys. Rev. D **65** (2002) 073031 [arXiv:hep-ph/0110307]; G. L. Fogli, G. Lettera, E. Lisi, A. Marrone, A. Palazzo and A. Rotunno, Phys. Rev. D **66**, 093008 (2002) [arXiv:hep-ph/0208026]; M. C. Gonzalez-Garcia and C. Pena-Garay, Phys. Rev. D **68**, 093003 (2003) [arXiv:hep-ph/0306001].
- [30] S. Choubey, S. Goswami and D. P. Roy, Phys. Rev. D **65** (2002) 073001 [arXiv:hep-ph/0109017]; S. Choubey, S. Goswami, N. Gupta and D. P. Roy, Phys. Rev. D **64** (2001) 053002 [arXiv:hep-ph/0103318].
- [31] C. Athanassopoulos *et al.*, (The LSND Collaboration) Phys. Rev. Lett. **77**, 3082 (1996); C. Athanassopoulos *et al.*, (The LSND Collaboration) Phys. Rev. Lett. **81**, 1774 (1998).
- [32] For an exhaustive list of reference for analysis including sterile neutrinos see [http : //www.nu.to.infn.it/Sterile\\_Neutrinos/](http://www.nu.to.infn.it/Sterile_Neutrinos/).

- [33] An incomplete list of relevant references includes:: V. D. Barger, D. Marfatia and K. Whisnant, Phys. Rev. Lett. **88**, 011302 (2002) [arXiv:hep-ph/0106207]; A. Bandyopadhyay, S. Choubey, S. Goswami and D. P. Roy, Mod. Phys. Lett. A **17**, 1455 (2002) [arXiv:hep-ph/0203169]; J. N. Bahcall, M. C. Gonzalez-Garcia and C. Pena-Garay, Phys. Rev. C **66**, 035802 (2002) [arXiv:hep-ph/0204194]; P. C. de Holanda and A. Y. Smirnov, arXiv:hep-ph/0211264; M. Maltoni, T. Schwetz, M. A. Tortola and J. W. F. Valle, Phys. Rev. D **67**, 013011 (2003) [arXiv:hep-ph/0207227].
- [34] J. Formaggio, talk at *5th International Workshop on Neutrino Factories & Superbeams*, NuFact '03, Columbia University, New York, 5-11 June 2003; <http://www.cap.bnl.gov/nufact03>.
- [35] M. Maris and S. T. Petcov, Phys. Rev. D **62**, 093006 (2000), (arXiv:hep-ph/0003301); G. L. Fogli, E. Lisi, D. Montanino and A. Palazzo, Phys. Rev. D **62**, 113003 (2000) [arXiv:hep-ph/0008012]; M. C. Gonzalez-Garcia, C. Pena-Garay and A. Y. Smirnov, Phys. Rev. D **63**, 113004 (2001), [arXiv:hep-ph/0012313].
- [36] G. Alimonti *et al.* [Borexino Collaboration], Astropart. Phys. **16**, 205 (2002) [arXiv:hep-ex/0012030].
- [37] S. Schönert, talk at Neutrino 2002, Munich, Germany, (<http://neutrino2002.ph.tum.de>).
- [38] A. Bandyopadhyay, S. Choubey and S. Goswami, Phys. Rev. D **67**, 113011 (2003) [arXiv:hep-ph/0302243].
- [39] J. N. Bahcall and C. Pena-Garay, JHEP **0311**, 004 (2003) [arXiv:hep-ph/0305159].
- [40] V. D. Barger, D. Marfatia and B. P. Wood, Phys. Lett. B **498**, 53 (2001) [arXiv:hep-ph/0011251]; H. Murayama and A. Pierce, Phys. Rev. D **65**, 013012 (2002) [arXiv:hep-ph/0012075]; A. de Gouvea and C. Pena-Garay, Phys. Rev. D **64**, 113011 (2001) [arXiv:hep-ph/0107186]; A. Bandyopadhyay, S. Choubey, R. Gandhi, S. Goswami and D. P. Roy, J. Phys. G **29**, 2465 (2003) [arXiv:hep-ph/0211266].
- [41] S. Choubey, S. T. Petcov and M. Piai, arXiv:hep-ph/0306017.
- [42] H. Robertson, talk at Eight international workshop on astroparticle and underground physics, TAUP 2003, Univ. of Washington, Seattle, Washington, September 5 - 9, 2003; <http://mocha.phys.washington.edu/taup2003/>.